Evidence for Quantum Stripe Ordering in a Triangular Optical Lattice

Xiao-Qiong Wang,[1,2,*] Guang-Quan Luo,[1,2,*] Jin-Yu Liu,[1,2] Guan-Hua Huang,[1,2] Zi-Xiang Li,[3] Congjun Wu,[4,5,6,7] Andreas Hemmerich,[8,†] and Zhi-Fang Xu[1,2,‡]

[1]*Department of Physics, Southern University of Science and Technology, Shenzhen 518055, China*
[2]*Shenzhen Institute for Quantum Science and Engineering, Southern University of Science and Technology, Shenzhen 518055, China*
[3]*Institute of Physics, Chinese Academy of Sciences, Beijing 100190, China*
[4]*New Cornerstone Science Laboratory, Department of Physics, School of Science, Westlake University, 310024 Hangzhou, China*
[5]*Institute for Theoretical Sciences, Westlake University, 310024 Hangzhou, China*
[6]*Key Laboratory for Quantum Materials of Zhejiang Province, Department of Physics, School of Science, Westlake University, Hangzhou 310030, China*
[7]*Institute of Natural Sciences, Westlake Institute for Advanced Study, Hangzhou 310024, China*
[8]*Institute of Quantum Physics, University of Hamburg, Luruper Chaussee 149, 22761 Hamburg, Germany*

(Received 10 November 2022; revised 16 January 2023; accepted 6 November 2023; published 27 November 2023)

Understanding strongly correlated quantum materials, such as high-T_c superconductors, iron-based superconductors, and twisted bilayer graphene systems, remains as one of the outstanding challenges in condensed matter physics. Quantum simulation with ultracold atoms in particular optical lattices, which provide orbital degrees of freedom, is a powerful tool to contribute new insights to this endeavor. Here, we report the experimental realization of an unconventional Bose-Einstein condensate of ^{87}Rb atoms populating degenerate p orbitals in a triangular optical lattice, exhibiting remarkably long coherence times. Using time-of-flight spectroscopy, we observe that this state spontaneously breaks the rotational symmetry and its momentum spectrum agrees with the theoretically predicted coexistence of exotic stripe and loop-current orders. Like certain strongly correlated electronic systems with intertwined orders, such as high-T_c cuprate superconductors, twisted bilayer graphene, and the recently discovered chiral density-wave state in kagome superconductors AV_3Sb_5 (A = K, Rb, Cs), the newly demonstrated quantum state, in spite of its markedly different energy scale and the bosonic quantum statistics, exhibits multiple symmetry breakings at ultralow temperatures. These findings hold the potential to enhance our comprehension of the fundamental physics governing these intricate quantum materials.

DOI: 10.1103/PhysRevLett.131.226001

Understanding the foundational principles of quantum matter is of central importance in both condensed matter and cold atom physics. A hallmark of phase diagrams of correlated quantum materials is the emergence of multiple intertwined electronic orders [1,2]. For example, in unconventional superconductors (SCs) [3], superconductivity is intertwined with multiple orders including antiferromagnetism [4], nematicity [5], pair-density wave [6], and stripe order [7], emerging at different temperature scales and doping concentrations. Similar intertwined orders with different broken symmetries are ubiquitous in correlated systems, including iron-based superconductors [8], twisted bilayer graphene [9,10], and kagome superconductors [11–17]. Unraveling the physics underlying these intertwined orders will lead to a significant leap in understanding the fundamental principles of exotic quantum states in general.

The microscopic mechanisms driving intertwined orders in quantum materials like cuprate and kagome superconductors are still widely unexplained. Unveiling their fundamental physics requires precise tuning of system parameters and appropriate methods to observe and discriminate different orders. This can be an exceedingly difficult task due to the vast complexities of solid-state quantum materials. In contrast, ultracold atom systems offer an unchallenged combination of precision and control with respect to a wide spectrum of physical properties like quantum statistics, lattice geometry, dimensionality, or interaction strength [18–21]. Unconventional lattice geometries, e.g., triangular [22,23], honeycomb [24–26], or kagome [27], have been realized. Techniques such as Floquet engineering [28] and the implementation of orbital degrees of freedom [29–31] enable investigations beyond conventional s-band physics. Hence, ultracold atoms can serve as a complementary platform for exploring intertwined orders, including nematicity, loop currents, and stripe order.

Here, we report the first experimental realization of a Bose-Einstein condensate (BEC) of neutral atoms in the

p orbitals of a triangular optical lattice. Through active cooling during the dissipative condensation dynamics, we are able to largely extend the coherence time, such that the metastable p-orbital [29–31] ground state is closely approached. Remarkably, the interplay between lattice frustration and orbital degeneracy gives rise to an exotic finite-momentum superfluid phase reminiscent of pair-density wave states in SCs [6,32]. It also spontaneously breaks the sixfold lattice rotational symmetry. Unequivocal evidence is observed using time-of-flight spectroscopy. The observed momentum spectra clearly confirm the quantum stripe phase and are consistent with its coexistence with a loop-current order, theoretically predicted for bosons in the p orbitals of the triangular lattice [33]. Note that loop-current order is proposed as a candidate for the pseudogap state in high-T_c cuprate SC [34], attracting immense attention in both theoretical [35] and experimental regards [36]. Nevertheless, despite a continuing quest during the past two decades, unequivocal experimental evidence for loop currents has not been found. Recently, possible signatures of loop currents were detected in bilayer graphene systems [37] and kagome SCs [11–13,16,17]. Thus, the experimentally realized quantum stripe phase is expected to capture aspects of a bosonic version of the intertwined orders in cuprate high-T_c SC and kagome SC AV_3Sb_5 ($A = \mathrm{K}$, Rb, Cs), which could provide new insights into the fundamental physics of these correlated quantum materials. Moreover, our findings show remarkable differences as compared to the chiral superfluidity obtained in square [38] and hexagonal bipartite optical lattices [26], where the lattice rotational symmetry is preserved and no bond currents arise between adjacent sites. This work also differs significantly from previous works where time-reversal symmetry (TRS) is broken at a single-particle level via applying a synthetic magnetic field [39–42] and, hence, it is not a surprise to obtain a nonzero circulating current [43]. The unconventional multiorbital superfluidity discussed in Ref. [44] with threefold rotational symmetry is not a near-equilibrium state of the system but rather a dynamical artifact. The symmetry breaking from C_6 to C_3 is due to the interaction during the time-of-flight expansion dynamics [45].

Our experiments use a BEC of rubidium atoms. The atoms are optically confined by a dipole trap and a two-dimensional triangular optical lattice. The dipole trap is created by adding potentials generated respectively from three noninterfering laser beams propagating within the xy plane, mutually intersecting at an angle of 120°. The lattice potential [shown in Fig. 1(a)] is formed by three interfering laser beams, polarized linearly along the z axis, and propagating in opposite directions with regard to the three dipole-trap laser beams. All beams have a wavelength λ of about 1,064 nm. This specific configuration ensures that the combined potential of the triangular lattice and the dipole trap practically maintains a sixfold rotational symmetry.

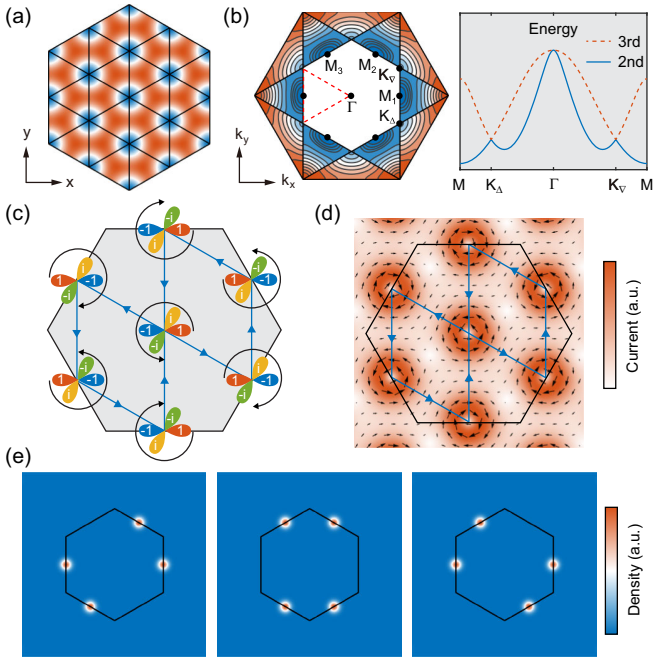

FIG. 1. Quantum stripe ordering for p-orbital bosons in a triangular optical lattice. (a) Lattice potential of the triangular optical lattice with maxima and minima shown by red and blue color, respectively. (b) The left-hand panel shows a contour plot of the second and third Bloch bands across the second and third Brillouin zones, respectively. The energy dispersion along the high symmetry lines forming the dashed red triangle is shown for both bands in the right-hand panel. The three inequivalent M points provide degenerate minima protected by the discrete rotational symmetry of the lattice. (c) Schematic order parameter of one of six possible implementations of the ground states within the second band. The gray hexagon denotes the unit cell of the order parameter. Each site contains an equal hybridization of two nonorthogonal p orbitals with a relative phase difference $\pm\pi/2$. The circular arrows illustrate the on-site orbital angular momentum. The solid blue lines with arrows denote the bond currents between nearest neighbor sites. (d) The corresponding mass current of the ground state. The amplitude (direction) of the current is shown by a color code (black arrows). (e) Momentum distributions of three representative ground states predicted theoretically. Solid black hexagons denotes the first Brillouin zone.

Focusing on the p-orbital Bloch bands of the lattice (i.e., the second and third bands), a triple-well scenario in the quasimomentum space arises in the second band, i.e., one finds three inequivalent energy minima of the second band, denoted M_1, M_2, M_3 in Fig. 1(b), located at the centers of the edges enclosing the first Brillouin zone. In our experiment we can adjust the second band energies $E_2(M_i)$, $i \in \{1, 2, 3\}$ at the M points via distortions of the unit cell (cf. Supplemental Material [46]). For the maximally symmetric case $E_2(M_1) = E_2(M_2) = E_2(M_3)$, theoretical considerations predict that the interaction among p-orbital bosons favors a metastable BEC [33], which equally populates two of three M points, and thus simultaneously breaks time-reversal symmetry and the sixfold lattice

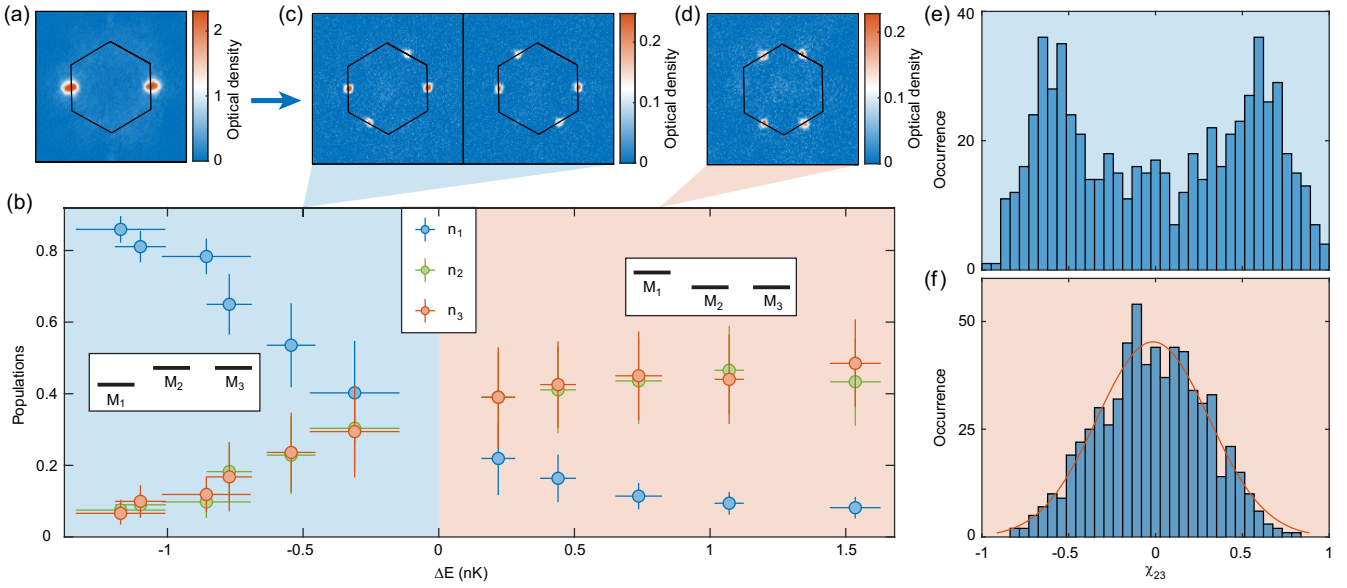

FIG. 2. Quantum phase transition induced by fine-tuning the energy imbalance. (a) The momentum distribution for the initial state, 0.1 ms after preparation of a condensate at M_1. (b) A distortion of the triangular lattice is applied to adjust the energy imbalance $\Delta E \equiv E_2(M_1) - [E_2(M_2) + E_2(M_3)]/2$ with equal energies $E_2(M_2) = E_2(M_3)$ maintained. The M-point populations after 130.1 ms evolution time, averaged over 111 experimental runs, is plotted versus ΔE. Error bars denote standard deviations. The insets illustrate the two characteristic configurations with respect to the M-point energies for $\Delta E < 0$ and $\Delta E > 0$. (c) Exemplary final state momentum distributions, recorded by time-of-flight measurements with $\Delta E \approx -0.5$ nK as indicated in the figure. (d) Same as (c), but with $\Delta E \approx 0.8$ nK. (e),(f) Histograms for the occurrence frequencies of the single-run values of χ_{23}, recorded after 140.1 ms holding time, for more than 600 runs with the same values of ΔE used in (c) and (d), respectively. The red solid line in (f) shows a Gaussian fit.

rotational symmetry accompanied by nonzero staggered loop currents. One of three possible implementations of the ground state in the second Bloch band is sketched in Fig. 1(c), which shows two p orbitals at each lattice site enclosing an angle of 60° superimposed with relative phases $\pm\pi/2$ leading to nonzero bond currents between nearest neighbor sites. The associated antiferromagnetic angular momentum is illustrated in Fig. 1(d). In Fig. 1(e), predicted momentum spectra of the three possible ground states are shown, each characterized by population peaks at different combinations of two M points.

We start with a bipartite hexagonal lattice, composed of two triangular lattices, slightly deformed such that the second band possesses a global minimum at a single M point (e.g., M_1). Details are found in Ref. [46]. This allows us to load a BEC into the second band at that M point by rapidly switching the relative potential offset ΔV between the two available classes of potential wells (cf. Ref. [26], Methods and Supplemental Material). By choosing the final value of ΔV appropriately, we ensure that, in configuration space, predominantly the s orbitals of the shallow wells are occupied. As discussed in Refs. [31,38], this keeps band relaxation collisions at a low level. In a second, adiabatic step, one of the triangular lattices is completely turned off such that the atoms in configuration space are transferred to the p orbitals of the other triangular lattice, while in regard to momentum space, they remain localized at the chosen M_1 point. Once the p orbitals are populated, increased band relaxation and associated heating sets in. After preparation of the BEC at the M_1 point shown in Fig. 2(a), the system is allowed to relax to its ground state. In order to maintain the phase coherence necessary to form the theoretically predicted quantum stripe ordering [33], we continuously cool the system by evaporation at the cost of extra atom loss.

We first simplify the symmetry breaking process necessary to reach one of degenerate ground states in the limited phase coherence time. Therefore, the degeneracy of the M points is partly lifted by inducing a small power imbalance of the three laser beams forming the triangular lattice. We fine-tune the energy imbalance $\Delta E \equiv E_2(M_1) - [E_2(M_2) + E_2(M_3)]/2$ while maintaining the degeneracy of M_2 and M_3 with $E_2(M_2) = E_2(M_3)$. Figure 2(b) records the averaged condensate populations n_j at M_j with $j = 1, 2, 3$ and $\sum_j n_j = 1$ after 130.1 ms holding time obtained from momentum distributions recorded via time-of-flight measurements. Starting from large and negative ΔE, interactions then favor almost all atoms condensing at M_1 with tiny populations at the other two M points. With increasing ΔE, the average population for atoms at M_1 monotonically decreases and the populations at M_2 and M_3 increase accordingly with equal average values. Characteristic momentum distributions for negative and positive values of ΔE are shown in Figs. 2(c) and 2(d).

When $\Delta E < 0$, we find that the atoms prefer to condense at two out of three M points with the majority of the atoms

populating the M_1 point with lower energy, and the minority of the atoms residing at the higher energy of one of the two degenerate M_2 or M_3 points. This is consistent with the histogram shown in Fig. 2(e), where a double peak structure appears for the population imbalance given by $\chi_{23} \equiv (n_2 - n_3)/(n_2 + n_3)$ and a negative correlation among atoms populating the M_2 and M_3 points arises. This indicates that a spontaneous symmetry breaking emerges due to interactions among p-orbital atoms. For the other case with $\Delta E > 0$, a different scenario occurs. We observe that the majority of atoms prefers to condense at the two lower energy points M_2 and M_3 with almost equal populations in each single run. This corresponds to the histogram for χ_{23} shown in Fig. 2(f), where a Gaussian profile with a maximum value at zero is obtained and a positive correlation among atoms residing at M_2 and M_3 is found. Based on these experimental results with moderate $|\Delta E|$, the interactions are found to favor the majority of the atoms to condense at two out of three M points. We thus expect that in the limit of $\Delta E \to 0$, this feature should persist. Theoretically, a first order quantum phase transition occurs when we cross $\Delta E = 0$. Details can be found in Ref. [46]. The main feature shown in Fig. 2 is consistent with this prediction. At zero temperature the populations are expected to undergo a discontinuity. Because of the finite temperature, in the experiment this jump is replaced by a continuous transition within a small region of $|\Delta E|$ of a few nanokelvin.

We next consider the maximally symmetric case with three degenerate minima of the second band at the three M points. Theoretical calculations suggest that the atoms should condense at two out of three degenerate Bloch states Φ_j with $\pm\pi/2$ phase difference, selected in a spontaneous symmetry breaking process. The plots in Fig. 1(e) show the theoretically predicted atomic momentum distributions for different ground states. To explore the predicted quantum stripe order, we carefully adjust the energy imbalance ΔE by changing the laser power of three beams and applying parametric heating to calibrate its value. However, this method has limitations with regard to the accuracy. Especially for the balanced case, tiny differences are hard to be precisely calibrated. Nevertheless, we roughly estimated $|\Delta E| \leq 0.3$ nK. We thus record the momentum distributions for atoms relaxing in the p orbitals for various holding times. Our experiments show two different timescales. First, in a relatively short time interval of about 40 ms, the system quickly thermalizes to states with approximately equal populations at three M points. Subsequently, slow evaporation dynamics further cools the system and drives it into lower energy states. These are shown in Ref. [46]. Figure 3(a) shows the statistical distribution of the final states after 140.1 ms holding time. Each dark red dot represents one of 636 experimental runs, specifying the populations n_1, n_2 of the points M_1 and M_2 using an oblique coordinate system.

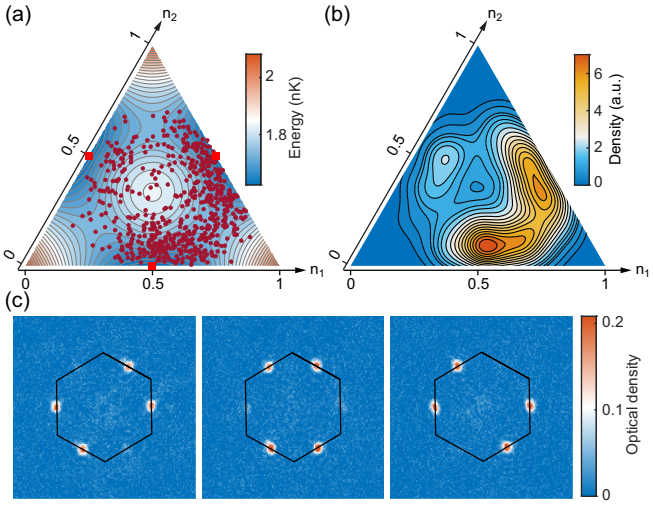

FIG. 3. Statistical analysis of the quantum stripe phase. (a) Statistical distribution of the final states at 140.1 ms holding time for 636 experimental runs. Each dark red dot shows the tuple (n_1, n_2) of populations of the points M_1 and M_2 using an oblique coordinate system. The mean-field energy per atom calculated via choosing optimized relative phases between condensates at three M points is shown by the color code and contour lines. Three red squares indicate the locations of the theoretically predicted ground states. The corresponding energy scale for the tunneling between two nearest neighbor p orbitals is about 8 nK. (b) The kernel density estimation of the data shown in (a), where three local maxima appear close to the predicted ground states, respectively. (c) Momentum distribution for the final states observed close to the three local maxima in the kernel density distribution shown in (b).

The mean-field energy per atom, calculated via choosing optimized relative phases between condensates at three M points, is shown by the color code and contour lines [46]. Three red squares indicate the locations of the theoretically predicted ground states. We apply a nonparametric kernel density estimation method to the data in Fig. 3(a), using the intrinsic function of MATLAB. The corresponding density distribution is shown in Fig. 3(b). A deep local minimum emerges close to the center of the triangle, which indicates that interaction does not favor equal populations of all three M points leading to lattice rotational symmetry breaking. However, three local maxima for the distribution are found to be close to the middle points of the three edges of the triangle [see red squares in Fig. 3(a)], which are the locations of the theoretical predicted ground states. Corresponding to the three maxima in the distribution in Fig. 3(b), three exemplary momentum distributions for the final states are shown in Fig. 3(c), which well reproduce the theoretical predicted momentum spectra of the ground states shown in Fig. 1(e). These findings provide clear experimental evidence for the emergence of an unconventional BEC of p-orbital bosons in a triangular optical lattice, where two out of three M points are populated. Hence, we unambiguously show that threefold rotational

symmetry is spontaneously broken in our experiment. Meanwhile, a quantum stripe order is formed, since atoms condense at two different quasimomenta.

To determine whether the observed quantum stripe phase also breaks TRS depends upon information of the relative phase of the condensate fractions at the two M points. This typically requires the observation of interference, for example, similar to what has been reported for a bipartite square lattice in Ref. [47]. In the triangular lattice of this work, where persistent evaporation cooling is necessary to maintain a low temperature and phase coherence, such measurements are not easily possible. Nevertheless, we can partially infer the desired phase information from a simple mean-field consideration. It is reasonable to assume that after a long relaxation time the final state should have a lower interaction energy per particle than the initial state, where all atoms are condensed at the M_1 point. Our observations combined with mean-field calculations let us exclude the possibility that the phase difference between the condensates at the two M points is close to zero or π with the consequence of nonzero bond currents [46]. This gives a clear indication that the observed final states break TRS and show a loop-current order. However, a conclusion merely based upon observations requires extensive additional experimental efforts.

To conclude, we have obtained unequivocal evidence for the spontaneous rotational symmetry breaking of an unconventional BEC in the p orbitals of a triangular optical lattice. The observed momentum spectra, according to which the atoms predominantly choose to condense in two of three possible M points, agree with the theoretically predicted coexistence of a quantum stripe phase with a loop-current order. Observations combined with mean-field considerations indicate that the observed phase breaks TRS. In summary, the realized exotic phase implements a bosonic analog to the intertwined orders found in certain electronic condensed matter systems. The ability to mimic intertwined orders in a well-controlled environment offers an opportunity to deepen our understanding of the underlying physics in correlated quantum materials. The achieved long phase coherence in a pure p-orbital band could also pave the way to achieve the preparation of strongly correlated states with orbital degrees of freedom [48], for example, unconventional orbital Mott phases [30].

This work is supported by the National Key R&D Program of China (Grants No. 2022YFA1404103 and No. 2018YFA0307200), the Key-Area Research and Development Program of Guangdong Province (Grant No. 2019B030330001), NSFC (Grants No. 12274196 and No. U1801661), and funds from Guangdong province (Grants No. 2019QN01X087 and No. 2019ZT08X324). C. W. is supported by NSFC (Grants No. 12234016 and No. 12174317) and the New Cornerstone Science Foundation. A. H. acknowledges support by Cluster of Excellence CUI: Advanced Imaging of Matter of the Deutsche Forschungsgemeinschaft (DFG)–EXC 2056–Project No. 390715994.

*These authors contributed equally to this work.
†hemmerich@physnet.uni-hamburg.de
‡xuzf@sustech.edu.cn

[1] Eduardo Fradkin, Steven A. Kivelson, and John M. Tranquada, Colloquium: Theory of intertwined orders in high temperature superconductors, Rev. Mod. Phys. **87**, 457 (2015).
[2] Cyril Proust and Louis Taillefer, The remarkable underlying ground states of cuprate superconductors, Annu. Rev. Condens. Matter Phys. **10**, 409 (2019).
[3] B. Keimer, S. A. Kivelson, M. R. Norman, S. Uchida, and J. Zaanen, From quantum matter to high-temperature superconductivity in copper oxides, Nature (London) **518**, 179 (2015).
[4] D. J. Scalapino, A common thread: The pairing interaction for unconventional superconductors, Rev. Mod. Phys. **84**, 1383 (2012).
[5] R. M. Fernandes, A. V. Chubukov, and J. Schmalian, What drives nematic order in iron-based superconductors?, Nat. Phys. **10**, 97 (2014).
[6] Daniel F. Agterberg, J. C. Séamus Davis, Stephen D. Edkins, Eduardo Fradkin, Dale J. Van Harlingen, Steven A. Kivelson, Patrick A. Lee, Leo Radzihovsky, John M. Tranquada, and Yuxuan Wang, The physics of pair-density waves: Cuprate superconductors and beyond, Annu. Rev. Condens. Matter Phys. **11**, 231 (2020).
[7] J. M. Tranquada, B. J. Sternlieb, J. D. Axe, Y. Nakamura, and S. Uchida, Evidence for stripe correlations of spins and holes in copper oxide superconductors, Nature (London) **375**, 561 (1995).
[8] Qimiao Si, Rong Yu, and Elihu Abrahams, High-temperature superconductivity in iron pnictides and chalcogenides, Nat. Rev. Mater. **1**, 16017 (2016).
[9] Yuan Cao, Valla Fatemi, Shiang Fang, Kenji Watanabe, Takashi Taniguchi, Efthimios Kaxiras, and Pablo Jarillo-Herrero, Unconventional superconductivity in magic-angle graphene superlattices, Nature (London) **556**, 43 (2018).
[10] Eva Y. Andrei and Allan H. MacDonald, Graphene bilayers with a twist, Nat. Mater. **19**, 1265 (2020).
[11] Yu-Xiao Jiang *et al.*, Unconventional chiral charge order in kagome superconductor KV_3Sb_5, Nat. Mater. **20**, 1353 (2021).
[12] C. Mielke, D. Das, J.-X. Yin, H. Liu, R. Gupta, Y.-X. Jiang, M. Medarde, X. Wu, H. C. Lei, J. Chang, Pengcheng Dai, Q. Si, H. Miao, R. Thomale, T. Neupert, Y. Shi, R. Khasanov, M. Z. Hasan, H. Luetkens, and Z. Guguchia, Time-reversal symmetry-breaking charge order in a kagome superconductor, Nature (London) **602**, 245 (2022).
[13] Linpeng Nie, Kuanglv Sun, Wanru Ma, Dianwu Song, Lixuan Zheng, Zuowei Liang, Ping Wu, Fanghang Yu, Jian Li, Min Shan *et al.*, Charge-density-wave-driven electronic nematicity in a kagome superconductor, Nature (London) **604**, 59 (2022).
[14] He Zhao, Hong Li, Brenden R. Ortiz, Samuel M. L. Teicher, Takamori Park, Mengxing Ye, Ziqiang Wang, Leon Balents,

Stephen D. Wilson, and Ilija Zeljkovic, Cascade of correlated electron states in the kagome superconductor CsV_3Sb_5, Nature (London) **599**, 216 (2021).
[15] Hui Chen *et al.*, Roton pair density wave in a strong-coupling kagome superconductor, Nature (London) **599**, 222 (2021).
[16] Kun Jiang, Tao Wu, Jia-Xin Yin, Zhenyu Wang, M Zahid Hasan, Stephen D Wilson, Xianhui Chen, and Jiangping Hu, Kagome superconductors AV_3Sb_5 ($A = $ K, Rb, Cs), Natl. Sci. Rev. **10**, nwac199 (2022).
[17] Titus Neupert, M. Michael Denner, Jia-Xin Yin, Ronny Thomale, and M. Zahid Hasan, Charge order and superconductivity in kagome materials, Nat. Phys. **18**, 137 (2022).
[18] Immanuel Bloch, Ultracold quantum gases in optical lattices, Nat. Phys. **1**, 23 (2005).
[19] Maciej Lewenstein, Anna Sanpera, Veronica Ahufinger, Bogdan Damski, Aditi Sen(De), and Ujjwal Sen, Ultracold atomic gases in optical lattices: Mimicking condensed matter physics and beyond, Adv. Phys. **56**, 243 (2007).
[20] Christian Gross and Immanuel Bloch, Quantum simulations with ultracold atoms in optical lattices, Science **357**, 995 (2017).
[21] Florian Schäfer, Takeshi Fukuhara, Seiji Sugawa, Yosuke Takasu, and Yoshiro Takahashi, Tools for quantum simulation with ultracold atoms in optical lattices, Nat. Rev. Phys. **2**, 411 (2020).
[22] C. Becker, P. Soltan-Panahi, J. Kronjäer, S. Dörscher, K. Bongs, and K. Sengstock, Ultracold quantum gases in triangular optical lattices, New J. Phys. **12**, 065025 (2010).
[23] J. Struck, C. Ölschläger, R. Le Targat, P. Soltan-Panahi, A. Eckardt, M. Lewenstein, P. Windpassinger, and K. Sengstock, Quantum simulation of frustrated classical magnetism in triangular optical lattices, Science **333**, 996 (2011).
[24] P. Soltan-Panahi, J. Struck, P. Hauke, A. Bick, W. Plenkers, G. Meineke, C. Becker, P. Windpassinger, M. Lewenstein, and K. Sengstock, Multi-component quantum gases in spin-dependent hexagonal lattices, Nat. Phys. **7**, 434 (2011).
[25] Shengjie Jin, Wenjun Zhang, Xinxin Guo, Xuzong Chen, Xiaoji Zhou, and Xiaopeng Li, Evidence of Potts-nematic superfluidity in a hexagonal sp^2 optical lattice, Phys. Rev. Lett. **126**, 035301 (2021).
[26] Xiao-Qiong Wang, Guang-Quan Luo, Jin-Yu Liu, W. Vincent Liu, Andreas Hemmerich, and Zhi-Fang Xu, Evidence for an atomic chiral superfluid with topological excitations, Nature (London) **596**, 227 (2021).
[27] Gyu-Boong Jo, Jennie Guzman, Claire K. Thomas, Pavan Hosur, Ashvin Vishwanath, and Dan M. Stamper-Kurn, Ultracold atoms in a tunable optical kagome lattice, Phys. Rev. Lett. **108**, 045305 (2012).
[28] C. Weitenberg and J. Simonet, Tailoring quantum gases by Floquet engineering, Nat. Phys. **17**, 1342 (2021).
[29] Congjun Wu, Unconventional Bose–Einstein condensations beyond the "no-node" theorem, Mod. Phys. Lett. B **23**, 1 (2009).
[30] Xiaopeng Li and W. Vincent Liu, Physics of higher orbital bands in optical lattices: A review, Rep. Prog. Phys. **79**, 116401 (2016).
[31] T. Kock, C. Hippler, A. Ewerbeck, and A. Hemmerich, Orbital optical lattices with bosons, J. Phys. B **49**, 042001 (2016).
[32] D. F. Agterberg, M. Geracie, and H. Tsunetsugu, Conventional and charge-six superfluids from melting hexagonal Fulde-Ferrell-Larkin-Ovchinnikov phases in two dimensions, Phys. Rev. B **84**, 014513 (2011).
[33] C. Wu, W. V. Liu, J. Moore, and S. Das Sarma, Quantum stripe ordering in optical lattices, Phys. Rev. Lett. **97**, 190406 (2006).
[34] C. M. Varma, Non-Fermi-liquid states and pairing instability of a general model of copper oxide metals, Phys. Rev. B **55**, 14554 (1997).
[35] Sylvain Capponi, Congjun Wu, and Shou-Cheng Zhang, Current carrying ground state in a bilayer model of strongly correlated systems, Phys. Rev. B **70**, 220505(R) (2004).
[36] Philippe Bourges, Dalila Bounoua, and Yvan Sidis, Loop currents in quantum matter, C.R. Phys. **22**, 1 (2021).
[37] Jianpeng Liu and Xi Dai, Orbital magnetic states in moiré graphene systems, Nat. Rev. Phys. **3**, 367 (2021).
[38] Georg Wirth, Matthias Ölschläger, and Andreas Hemmerich, Evidence for orbital superfluidity in the p-band of a bipartite optical square lattice, Nat. Phys. **7**, 147 (2011).
[39] M. Aidelsburger, M. Atala, M. Lohse, J. T. Barreiro, B. Paredes, and I. Bloch, Realization of the Hofstadter Hamiltonian with ultracold atoms in optical lattices, Phys. Rev. Lett. **111**, 185301 (2013).
[40] Hirokazu Miyake, Georgios A. Siviloglou, Colin J. Kennedy, William Cody Burton, and Wolfgang Ketterle, Realizing the Harper Hamiltonian with laser-assisted tunneling in optical lattices, Phys. Rev. Lett. **111**, 185302 (2013).
[41] M. Aidelsburger, M. Lohse, C. Schweizer, M. Atala, J. T. Barreiro, S. Nascimbène, N. R. Cooper, I. Bloch, and N. Goldman, Measuring the Chern number of Hofstadter bands with ultracold bosonic atoms, Nat. Phys. **11**, 162 (2014).
[42] Colin J. Kennedy, William Cody Burton, Woo Chang Chung, and Wolfgang Ketterle, Observation of Bose–Einstein condensation in a strong synthetic magnetic field, Nat. Phys. **11**, 859 (2015).
[43] Marcos Atala, Monika Aidelsburger, Michael Lohse, Julio T. Barreiro, Belén Paredes, and Immanuel Bloch, Observation of chiral currents with ultracold atoms in bosonic ladders, Nat. Phys. **10**, 588 (2014).
[44] Parvis Soltan-Panahi, Dirk-Sören Lühmann, Julian Struck, Patrick Windpassinger, and Klaus Sengstock, Quantum phase transition to unconventional multi-orbital superfluidity in optical lattices, Nat. Phys. **8**, 71 (2011).
[45] M. Weinberg, O. Jürgensen, C. Ölschläger, D.-S. Lühmann, K. Sengstock, and J. Simonet, Symmetry-broken momentum distributions induced by matter-wave diffraction during time-of-flight expansion of ultracold atoms, Phys. Rev. A **93**, 033625 (2016).
[46] See Supplemental Materials at http://link.aps.org/supplemental/10.1103/PhysRevLett.131.226001 for additional details on state preparation and detection, single-particle band structure, tight-binding models, mean-field results, loop current, and domain structure.
[47] T. Kock, M. Ölschläger, A. Ewerbeck, W.-M. Huang, L. Mathey, and A. Hemmerich, Observing chiral superfluid order by matter-wave interference, Phys. Rev. Lett. **114**, 115301 (2015).
[48] Y. Tokura and N. Nagaosa, Orbital physics in transition-metal oxides, Science **288**, 462 (2000).